Supplementary Material: Quantifying the Fate of Wastewater Nitrogen Discharged to a Canadian River

Jason J. Venkiteswaran[*†] Sherry L. Schiff[‡] Brian P. Ingalls[§]

[*]Department of Geography and Environmental Studies, Wilfrid Laurier University, Waterloo, Ontario, Canada, N2L 3C5

[†]Corresponding author: jvenkiteswaran@wlu.ca

[‡]Department of Earth and Environmental Sciences, University of Waterloo, Waterloo, Ontario, Canada, N2L 3G1

[§]Department of Applied Mathematics, University of Waterloo, Waterloo, Ontario, Canada, N2L 3G1

1 Methods

1.1 Model Background

As is common in natural abundance stable isotope studies, isotopic ratios, $\text{Ratio} = \frac{^{15}\text{N}}{^{14}\text{N}}$, are measured and reported in δ notation, $\delta = \frac{\text{Ratio}_{\text{measured}}}{\text{Ratio}_{\text{N}_2}} - 1$ as deviations from atmospheric N_2 (defined as 0.0036765). Here, the concentration of the light isotope is assumed to approximate that of the bulk concentration (*conc*) and thus the concentration of the heavy isotope (hereafter as *iso*) is calculated as $iso = \text{Ratio} \times conc$.

As described in the main text, our initial model formulation describes the fate of ten species. For clarity they are written as:

$$\begin{aligned} &\text{NH}_3,\ \text{NH}_4{}^+,\ \text{NO}_2{}^-,\ \text{NO}_3{}^-,\ \text{N}_2\text{O} \\ &iso\text{NH}_3,\ iso\text{NH}_4{}^+,\ iso\text{NO}_2{}^-,\ iso\text{NO}_3{}^-,\ iso\text{N}_2\text{O} \end{aligned}$$

involved in fourteen reactions with rate constants as follows:

$$\begin{aligned} k_1 &: \quad \text{NH}_3 \rightarrow \text{NH}_4{}^+ \\ \alpha_1 k_1 &: \quad iso\text{NH}_3 \rightarrow iso\text{NH}_4{}^+ \\ k_2 &: \quad \text{NH}_4{}^+ \rightarrow \text{NH}_3 \\ \alpha_2 k_2 &: \quad iso\text{NH}_4{}^+ \rightarrow iso\text{NH}_3 \\ k_{ge} &: \quad \text{NH}_3 \rightarrow \\ \alpha_{ge} k_{ge} &: \quad iso\text{NH}_3 \rightarrow \\ k_{amup} &: \quad \text{NH}_4{}^+ \rightarrow \\ \alpha_{amup} k_{amup} &: \quad iso\text{NH}_4{}^+ \rightarrow \\ k_{nit1} &: \quad \text{NH}_4{}^+ \rightarrow \text{NO}_2{}^- \\ \alpha_{nit1} k_{nit1} &: \quad iso\text{NH}_4{}^+ \rightarrow iso\text{NO}_2{}^- \\ k_{nit2} &: \quad \text{NO}_2{}^- \rightarrow \text{NO}_3{}^- \\ \alpha_{nit2} k_{nit2} &: \quad iso\text{NO}_2{}^- \rightarrow iso\text{NO}_3{}^- \\ k_{denit} &: \quad \text{NO}_3{}^- \rightarrow \text{N}_2\text{O} \\ \alpha_{denit} k_{denit} &: \quad iso\text{NO}_3{}^- \rightarrow iso\text{N}_2\text{O} \end{aligned}$$

characterized by fourteen free kinetic parameters. Note that the states N_2O and $iso N_2O$ do not contribute to the dynamics; they are sink species.

Observations were available through four outputs:

$$[NH_3] + [NH_4^+]$$
$$[NO_3^-]$$
$$[\delta^{15}N{-}NH_3] + [\delta^{15}N{-}NH_4^+]$$
$$[\delta^{15}N{-}NO_3^-].$$

1.2 Preliminary Analysis

In impacted rivers, nitrogen (N) cycle processes of nitrification, denitrification, uptake, and gas exchange all occur simultaneously complicating interpretation of nitrogen concentrations and isotopes. The effect of individual processes was explored with the model by initializing the model with typical field conditions and allowing the N to evolve with time. The resultant curves show the similarity and differences among the individually modelled processes. In turn, it is these differences that allow the model to search for unique solutions (Supplementary Figures 1–4).

1.3 Model Reduction

An initial structural identifiability analysis[1] of the model dynamics and outputs confirmed that with data collected through these output channels, it would not be possible to estimate (i) the rates of transfer between NH_3 and NH_4^+ and $iso NH_3$ and $iso NH_4^+$ (i.e. the values of parameters k_1, k_2, α_1, α_2) nor (ii) separately the rates at which the equilibrated NH_3/NH_4^+ and $iso NH_3/iso NH_4^+$ pools are depleted through the volatilization (k_{ge}) and biological assimilation (k_{amup}) processes.

Consequently, we simplified the model as follows. First, we fixed the rates of k_{ge} from[5,9] and the scaling factor α_{ge} from[6–8] to the values $k_{ge} = 0.002$ $t^{-1}m^{-1}$, $\alpha_{ge} = 0.995$. Second, we lumped the ammonia species NH_3/NH_4^+ and $iso NH_3/iso NH_4^+$ into equilibrated pools (called TAN and isoTAN, respectively), whose distribution is set by pH readings, as follows. We set

$$f_{NH_3} = \frac{10^{-9.25}/10^{-pH}}{1 + 10^{-9.25}/10^{-pH}}$$

where f_{NH_3} is the fraction of TAN or isoTAN in the NH_3 state and pH is the mean of all pH measurements associated with each dataset. These

simplifications resulted in a model (Figure 2) with eight states

$$[\mathrm{TAN}],\ [\mathrm{NO_2}^-],\ [\mathrm{NO_3}^-],\ [\mathrm{N_2O}]$$
$$[iso\mathrm{TAN}],\ [iso\mathrm{NO_2}^-],\ [iso\mathrm{NO_3}^-],\ [iso\mathrm{N_2O}]$$

involved in ten reactions:

$$\begin{aligned}
&k_{ge}: \quad \mathrm{NH_3} \rightarrow \\
&\alpha_{ge}k_{ge}: \quad iso\mathrm{NH_3} \rightarrow \\
&k_{amup}: \quad \mathrm{NH_4}^+ \rightarrow \\
&\alpha_{amup}k_{amup}: \quad iso\mathrm{NH_4}^+ \rightarrow \\
&k_{nit1}: \quad \mathrm{NH_4}^+ \rightarrow \mathrm{NO_2}^- \\
&\alpha_{nit1}k_{nit1}: \quad iso\mathrm{NH_4}^+ \rightarrow iso\mathrm{NO_2}^- \\
&k_{nit2}: \quad \mathrm{NO_2}^- \rightarrow \mathrm{NO_3}^- \\
&\alpha_{nit2}k_{nit2}: \quad iso\mathrm{NO_2}^- \rightarrow iso\mathrm{NO_3}^- \\
&k_{denit}: \quad \mathrm{NO_3}^- \rightarrow \mathrm{N_2O} \\
&\alpha_{denit}k_{denit}: \quad iso\mathrm{NO_3}^- \rightarrow iso\mathrm{N_2O}
\end{aligned}$$

characterized by eight unknown kinetic parameters. Here $\mathrm{NH_3} = f_{\mathrm{NH_3}} \times \mathrm{TAN}$, $\mathrm{NH_4}^+ = (1 - f_{\mathrm{NH_3}}) \times \mathrm{TAN}$, and likewise for $iso\mathrm{NH_3}$ and $iso\mathrm{NH_4}^+$.

As described in the main text, we used simecol to fit this model separately to the four available data sets (Figures 3-6). We confirmed these results by implementing the fitting algorithm in MATLAB (Mathworks) (simulation with `ode23s`, fitting with `simulannealbnd` and `fmincon`, details below). We then applied uncertainty analysis as described below to each model fit. From this preliminary analysis (results not shown) we determined that in every case the available data was not sufficient to provide accurate estimates of the eight free parameters. In particular, the values of k_{nit2} and α_{nit2} could not be well-estimated from any of the datasets. Consequently, we reduced the model further, by describing nitrification as a single-step process by removing the nitrate $\mathrm{NO_2}^-$ population and describing a single process by which $\mathrm{NH_4}^+$ is converted to $\mathrm{NO_3}^-$, with kinetics described by k_{nit1} and α_{nit1}. The resulting model has six states:

$$[\mathrm{TAN}],\ [\mathrm{NO_3}^-],\ [\mathrm{N_2O}]$$
$$[iso\mathrm{TAN}],\ [iso\mathrm{NO_3}^-],\ [iso\mathrm{N_2O}]$$

Again, $\mathrm{N_2O}$ and $iso\mathrm{N_2O}$ do not contribute to the dynamics, they are simply sinks, so this could be formulated as a four-state model. The eight remaining

processes are:

$$
\begin{aligned}
k_{ge}: &\quad \mathrm{NH_3} \rightarrow \\
\alpha_{ge}k_{ge}: &\quad iso\mathrm{NH_3} \rightarrow \\
k_{amup}: &\quad \mathrm{NH_4}^+ \rightarrow \\
\alpha_{amup}k_{amup}: &\quad iso\mathrm{NH_4}^+ \rightarrow \\
k_{nit1}: &\quad \mathrm{NH_4}^+ \rightarrow \mathrm{NO_2}^- \\
\alpha_{nit1}k_{nit1}: &\quad iso\mathrm{NH_4}^+ \rightarrow iso\mathrm{NO_2}^- \\
k_{denit}: &\quad \mathrm{NO_3}^- \rightarrow \mathrm{N_2O} \\
\alpha_{denit}k_{denit}: &\quad iso\mathrm{NO_3}^- \rightarrow iso\mathrm{N_2O}
\end{aligned}
$$

characterized by six free variables. The results of our uncertainty analysis of this model are shown in figures S4-S7, and are summarized in the main text.

1.4 Model Calibration and Uncertainty Analysis

Calibration: Measurement error was estimated for each of the observations as follows. For light isotope concentrations, the standard deviation of measurement error was presumed fixed at 0.1 mgN/L. For the light isotopes, the assigned standard deviation is δ^{15}N-$\mathrm{NO_3}^-$ is 0.3‰ and on the δ^{15}N-TAN is 0.5‰. The standard deviation of error in concentrations is then determined as

$$
\left([conc] \left(\frac{\delta}{1000} + 1 \right) \times 0.0036765 \sqrt{ \left(\frac{0.1}{[conc]} \right)^2 + \left(\frac{\epsilon}{1000} / \left(\frac{\delta}{1000} + 1 \right) \right)^2 } \right)^2
$$

where $[conc]$ is the corresponding light isotope concentration, 0.0036765 is the isotopic ratio of atmospheric $\mathrm{N_2}$ gas, ϵ is 0.3 for $\delta^{15}\mathrm{N}-\mathrm{NO_3}^-$ and 0.5 for $\delta^{15}\mathrm{N}-\mathrm{TAN}$, and δ is the observed delta value.

We calibrated the model by minimizing the weighted sum of squares function:

$$
SSE(\mathbf{p}) = \sum_i \sum_k \frac{\left(y^i_{obs}(t_k) - y^i_{sim}(\mathbf{p}, t_k) \right)^2}{(\sigma^i(t_k)^2} \tag{1}
$$

where $y^i_{obs}(t_k)$ is the measurement from output channel i at time t_k, $\sigma^j(t_k)$ is the corresponding estimate of the standard deviation of the error, and

$y^i_{sim}(\mathbf{p}, t_k)$ is the model prediction of output i at time t_k. The four output channels are [TAN], [$NO_3{}^-$], δ^{15}N−TAN, and δ^{15}N−$NO_3{}^-$. For each dataset, the SSE was minimized over the corresponding parameter space by application of global optimization routines (simulated annealing, through the MATLAB function `simannealbnd`) and interior point method, through the MATLAB function `fmincon`). Multiple starting points were employed to avoid local minima. Parameter values were bound to the range $[0, 50]$ for k values and $[0.975, 1]$ for alpha values. The initial concentrations were allowed to be free parameters, to avoid over-weighting the measurements at these points. Best fit parameter sets are reported in Tables S4-S7.

Sensitivity Analysis

For each dataset, local absolute sensitivity coefficients were determined at the best-fit parametrization

$$S_{i,j}(t_k) = \left.\frac{\partial y^i_{sim}(\mathbf{p}, t_k)}{\partial p_j}\right|_{t=t_k}$$

where $y^j_{sim}(\mathbf{p}, t_k)$ is the i-th model output at time t_k and p_j is the j-th parameter. Derivatives were approximated by finite differences of 1% in the parameter p_j. Scaling of these absolute sensitivity coefficients yields dimensionless relative sensitivity measures:

$$\tilde{S}_{i,j}(t_k) = \frac{p_j}{y^i_{sim}(\mathbf{p}, t_k)} \tilde{S}_{i,j}(t_k).$$

These relative sensitivities were used to gauge the strength of each model parameter on the model's predictions of the observations:[2]

$$S_j = \sqrt{\frac{1}{m} \sum_{k=1} \sum_{i=1} [\tilde{S}_{i,j}(t_k)]^2}$$

where i runs over all output channels, and t_k runs over all corresponding observation timepoints.

Practical Identifiability

We then applied the orthogonalization approach of[10] to arrive at practical measures of identifiability, as follows. The relative sensitivity coefficients for each parameter were arranged in columns to generate a sensitivity

coefficient matrix:

$$\mathbf{S} = \begin{bmatrix} \tilde{S}_{1,1}(t_1) & \cdots & \tilde{S}_{1,n_p}(t_1) \\ \vdots & \ddots & \vdots \\ \tilde{S}_{n_o,1}(t_1) & \cdots & \tilde{S}_{n_o,n_p}(t_1) \\ \tilde{S}_{1,1}(t_2) & \cdots & \tilde{S}_{1,n_p}(t_2) \\ \vdots & \ddots & \vdots \\ \tilde{S}_{n_0,1}(t_{n_T}) & \cdots & \tilde{S}_{n_0,n_p}(t_{n_T}) \end{bmatrix}$$

where there are n_p parameters, n_o observables, and n_T timepoints. (Entries corresponding to missing timepoints were set to zero.) The column with the largest sum of squared entries was labeled $\mathbf{X}_1$; it corresponds to the parameter with the highest identifiability score. Each column of $\mathbf{S}$ was then projected onto $\mathbf{X}_1$, and the residuals were collected in matrix $\mathbf{R}_1$:

$$\mathbf{R}_1 = \mathbf{S} - \mathbf{X}_1(\mathbf{X}_1^T\mathbf{X}_1)^{-1}\mathbf{X}_1^T\mathbf{S}$$

The column of $\mathbf{R}_1$ with the largest sum of squares was found as the next most identifiable parameter. The matrix $\mathbf{X}_1$ was then concatenated with the corresponding column of $\mathbf{S}$ to form $\mathbf{X}_2$. The residuals of the projection of $\mathbf{S}$ onto $\mathbf{X}_2$ were then calculated, and the third most identifiable parameter was identified. This process was iterated to provide an identifiability score for each parameter: the 2-norm (square root of sum of squared entries) of the corresponding column vector of matrix $\mathbf{X}_j$. These identifiability scores are reported in Tables S4-S7.

Confidence Intervals

Following,[3,4] we estimated confidence intervals for the best fit parameter estimates by first constructing the Fisher Information Matrix:

$$\text{FIM} = \mathbf{S}^T\mathbf{W}\mathbf{S}$$

where $\mathbf{W}$ is the inverse of the measurement covariance matrix. Then assuming the measurement errors are independent and normally distributed, the Cramer-Rao bound establishes a lower bound on the variance of the parameter estimates of

$$\sigma^2(p_j) \geq (\text{FIM}^{-1})_{jj} \tag{2}$$

A lower bound on the size of a 95% confidence interval is then given by

$$1.96\sigma(p_j)$$

These confidence estimates are reported in Tables S4-S7.

The sensitivity measure gives a preliminary description of the degree to which a parameter's value impacts the observed behaviour. Low sensitivities correspond to parameters that are not well-constrained by the observed data. Identifiability scores take sensitivity into account, and further account for the degree of correlation among the parameters' effects. Parameters with low identifiability scores are less well-constrained by the available data. The 95% confidence values must be interpreted carefully: they are lower bounds on the relative size of 95% confidence intervals under the assumptions that errors are independent and normally distributed and model mismatch is caused solely by measurement error (i.e. the model is 'correct'); both conditions are only approximately true here. Nevertheless, small confidence intervals suggest more accurate parameter estimates.

References

[1] R. Bellman and K. Åström. On structural identifiability. *Mathematical Biosciences*, 7(3):329 – 339, 1970.

[2] R. Brun, M. Kühni, H. Siegrist, W. Gujer, and P. Reichert. Practical identifiability of {ASM2d} parameters—systematic selection and tuning of parameter subsets. *Water Research*, 36(16):4113 – 4127, 2002.

[3] A. F. Emery and A. V. Nenarokomov. Optimal experiment design. *Measurement Science and Technology*, 9(6):864, 1998.

[4] K. G. Gadkar, R. Gunawan, and F. J. Doyle. Iterative approach to model identification of biological networks. *BMC Bioinformatics*, 6(1):1, 2005.

[5] T. S. Jamieson, S. L. Schiff, and W. D. Taylor. Using stable isotopes of dissolved oxygen for the determination of gas exchange in the Grand River, Ontario, Canada. *Water Research*, 47(2):781 – 790, 2013.

[6] I. Kirshenbaum, J. S. Smith, T. Crowell, J. Graff, and R. McKee. Separation of the Nitrogen Isotopes by the Exchange Reaction between Ammonia and Solutions of Ammonium Nitrate. *The Journal of Chemical Physics*, 15(7):440–446, 1947.

[7] E. Norlin, K. Irgum, and K. E. A. Ohlsson. Determination of the $^{15}N/^{14}N$ ratio of ammonium and ammonia in aqueous solutions by equilibrium headspace-gas chromatography-combustion-isotope ratio mass spectrometry. *The Analyst*, 127(6):735–740, 2002.

[8] H. G. Thode, R. L. Graham, and J. A. Ziegler. A Mass Spectrometer and the Measurement of Isotope Exchange Factors. *Canadian Journal of Research*, 23b(1):40–47, 1945.

[9] J. J. Venkiteswaran, S. L. Schiff, and W. D. Taylor. Linking aquatic metabolism, gas exchange, and hypoxia to impacts along the 300-km Grand River, Canada. *Freshwater Science*, 34(4):1216–1232, 2015.

[10] K. Z. Yao, B. M. Shaw, B. Kou, K. B. McAuley, and D. Bacon. Modeling ethylene/butene copolymerization with multi-site catalysts: parameter estimability and experimental design. *Polymer Reaction Engineering*, 11(3):563–588, 2003.

2 Figures

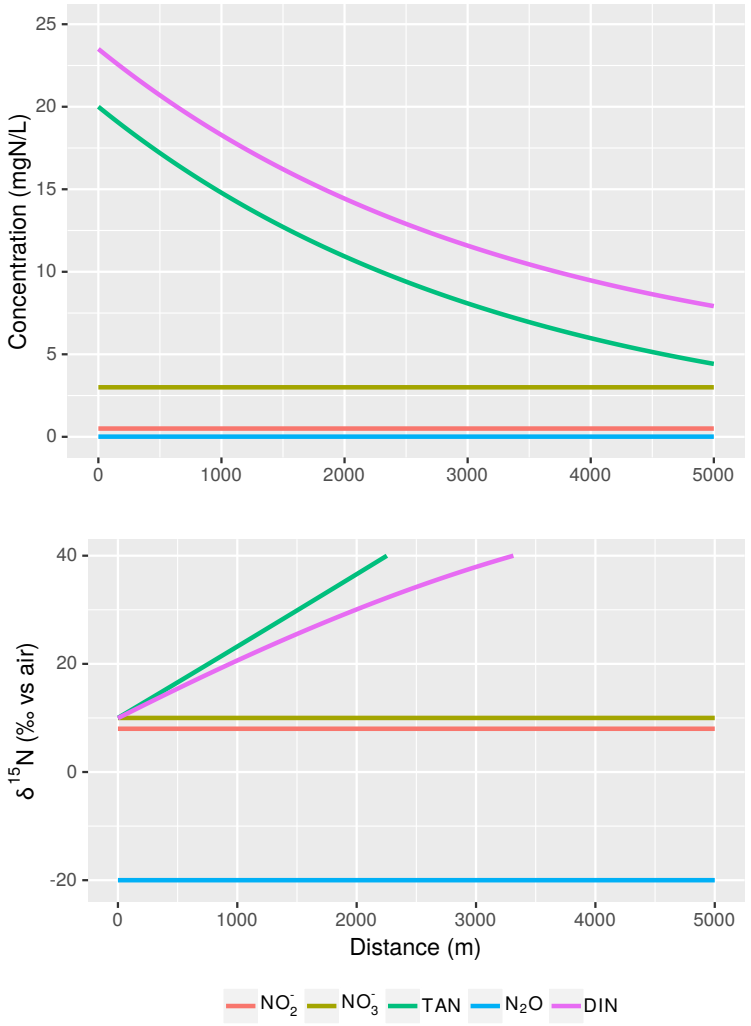

Figure S1: Each process imparts a different pattern in concentration and δ^{15}N values downstream of a WWTP discharge point in the *eight-state model*. Here, NH_3 volatilization only with $k_{ge} = 0.002$. Initial conditions were typical for the WWTPs under study: pH 8.5, temperature 20°C, TAN 20.0 mgN/L, NO_2^- 0.5 mgN/L, NO_3^- 3.0 mgN/L, N_2O 0.01 mgN/L, δ^{15}N-TAN +12.0‰, δ^{15}N-NO_2^- +8.0‰, δ^{15}N-NO_3^- +8‰, δ^{15}N-N_2O -20‰. Dissolved inorganic nitrogen (DIN = TAN + NO_2^- + NO_3^- and δ^{15}N-DIN is mass-weighted) is plotted to show where there is nitrogen loss from the system either through degassing, assimilation or denitrification.

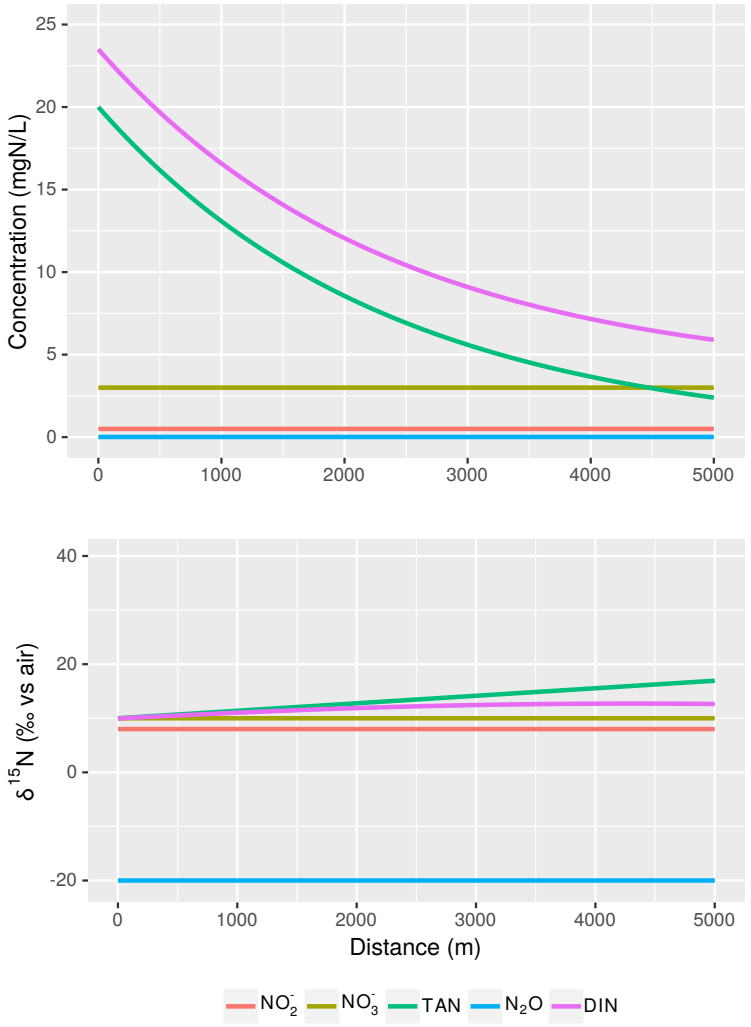

Figure S2: Each process imparts a different pattern in concentration and δ^{15}N values downstream of a WWTP discharge point in the *eight-state model*. Here, NH_4^+ uptake by biota only with $k_{amup} = 0.0005$ and $\alpha_{amup} = 0.990$. Initial conditions as per Figure S1.

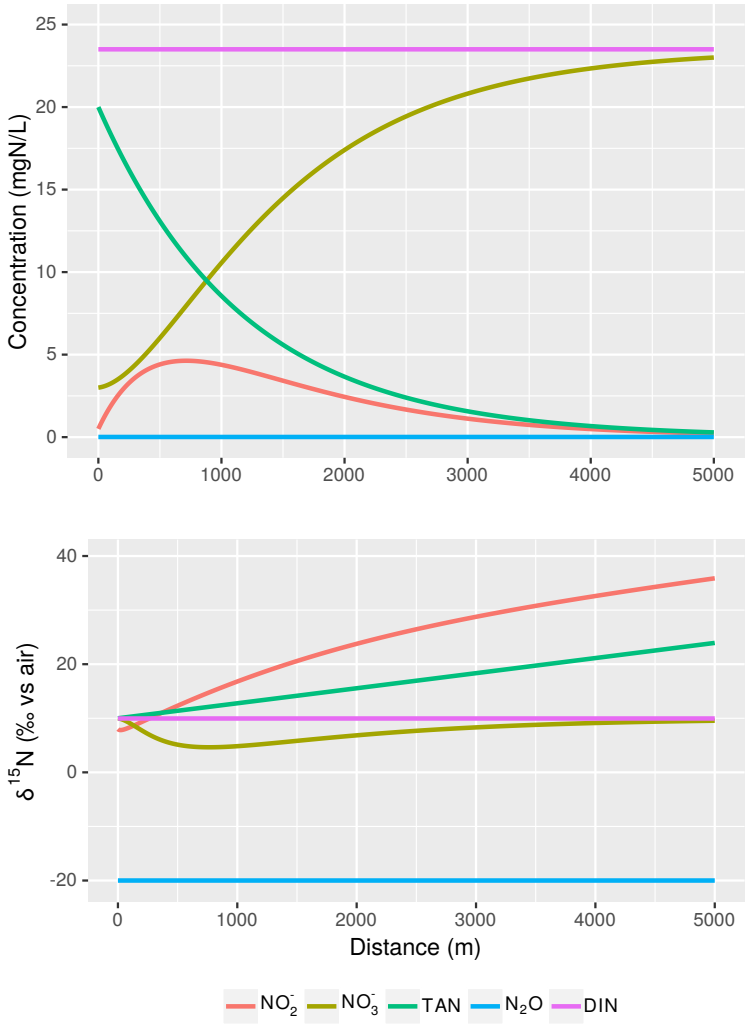

Figure S3: Each process imparts a different pattern in concentration and δ^{15}N values downstream of a WWTP discharge point in the *eight-state model*. Here, nitrification only with $k_{nit1} = 0.001$, $k_{nit1} = 0.002$, $\alpha_{nit1} = 0.990$, and $\alpha_{nit2} = 0.990$. Initial conditions as per Figure S1.

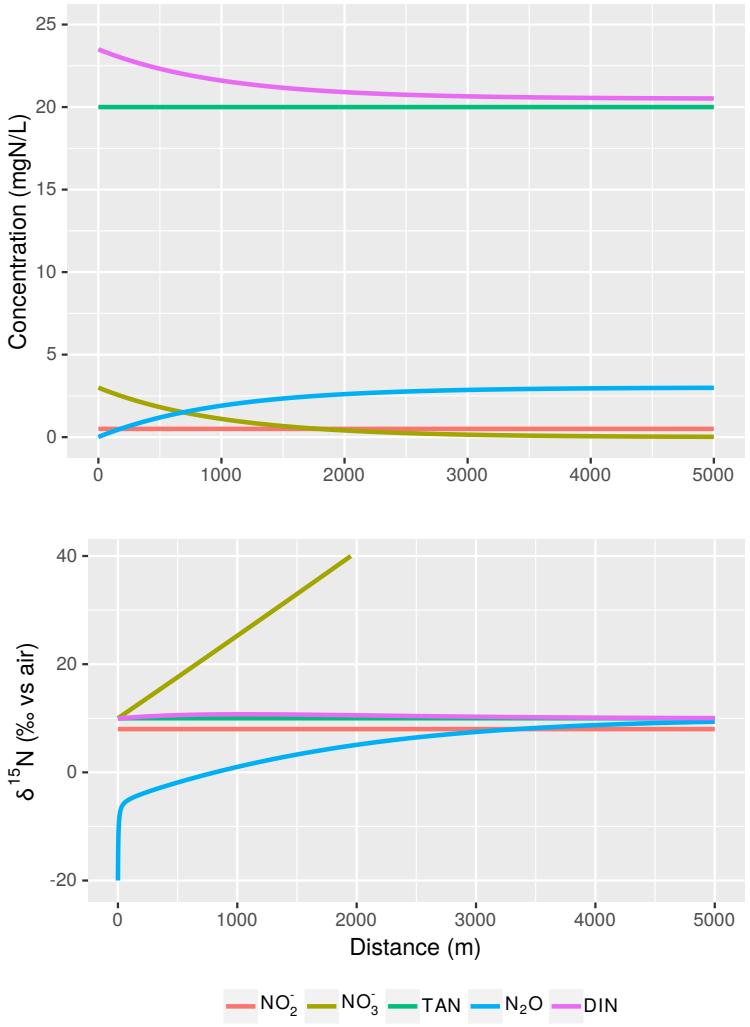

Figure S4: Each process imparts a different pattern in concentration and δ^{15}N values downstream of a WWTP discharge point in the *eight-state model*. Here, denitrification only with $k_{denit} = 0.001$ and $\alpha_{denit} = 0.985$. Initial conditions as per Figure S1.

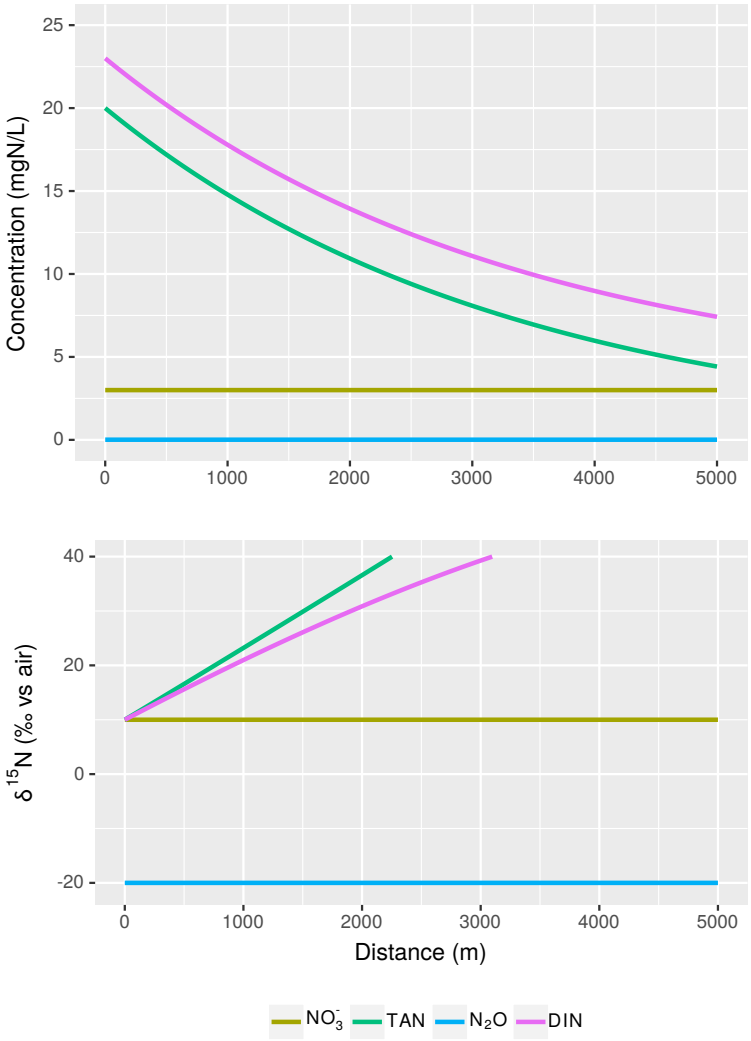

Figure S5: Each process imparts a different pattern in concentration and δ^{15}N values downstream of a WWTP discharge point in the *six-state model*. Here, NH_3 volatilization only with k_{ge} = 0.002. Initial conditions were typical for the WWTPs under study: pH 8.5, temperature 20°C, TAN 20.0 mgN/L, NO_3^- 3.0 mgN/L, N_2O 0.01 mgN/L, δ^{15}N-TAN +12.0‰, δ^{15}N-NO_3^- +8‰, δ^{15}N-N_2O -20‰. Dissolved inorganic nitrogen (DIN = TA + NO_3^- and δ^{15}N-DIN is mass-weighted) is plotted to show where there is nitrogen loss from the system either through degassing, assimilation or denitrification.

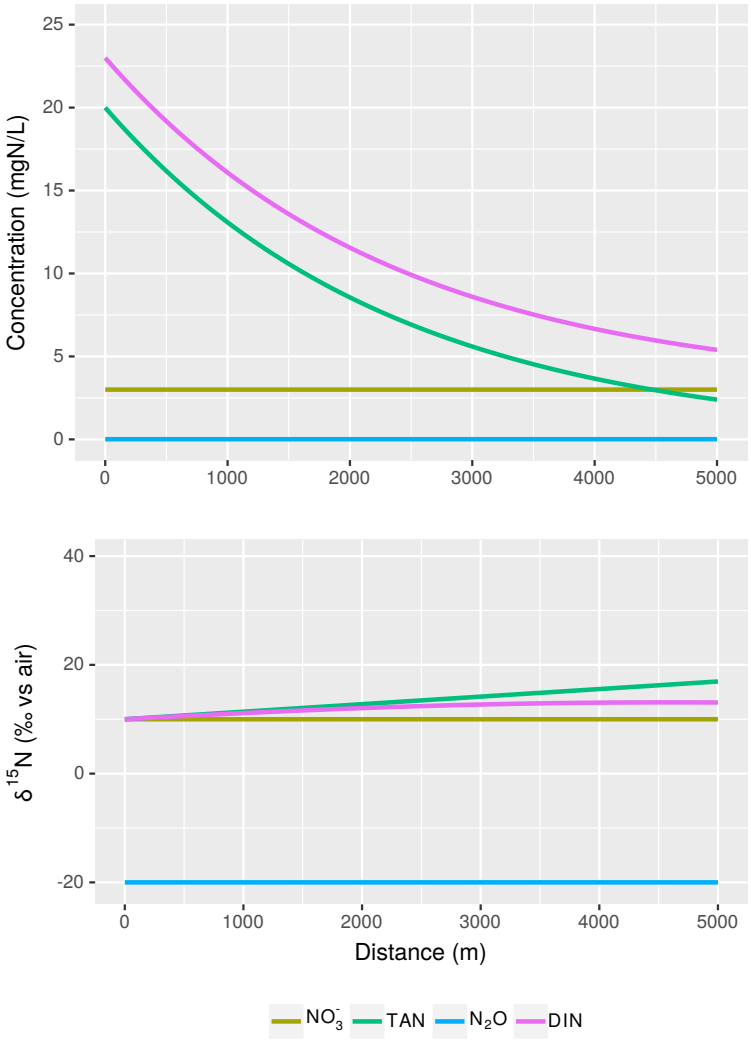

Figure S6: Each process imparts a different pattern in concentration and δ^{15}N values downstream of a WWTP discharge point in the *six-state model*. Here, NH_4^+ uptake by biota only with $k_{amup} = 0.0005$ and $\alpha_{amup} = 0.990$. Initial conditions as per Figure S5.

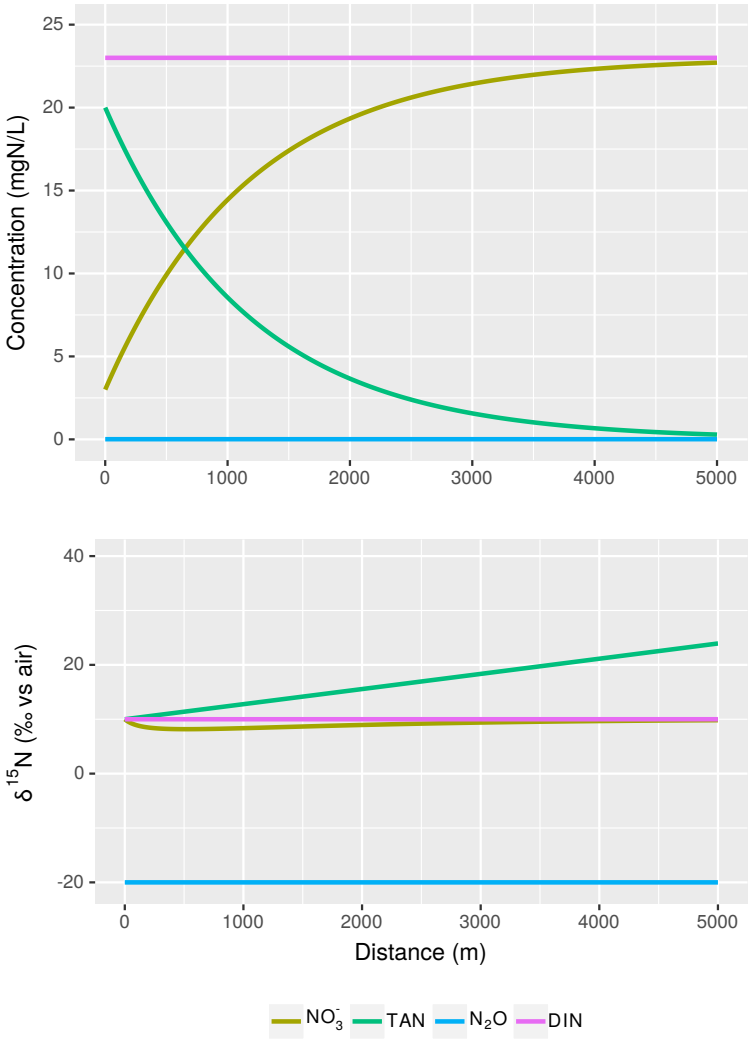

Figure S7: Each process imparts a different pattern in concentration and δ^{15}N values downstream of a WWTP discharge point in the *six-state model*. Here, nitrification only with $k_{nit1} = 0.001$ $\alpha_{nit1} = 0.990$. Initial conditions as per Figure S5.

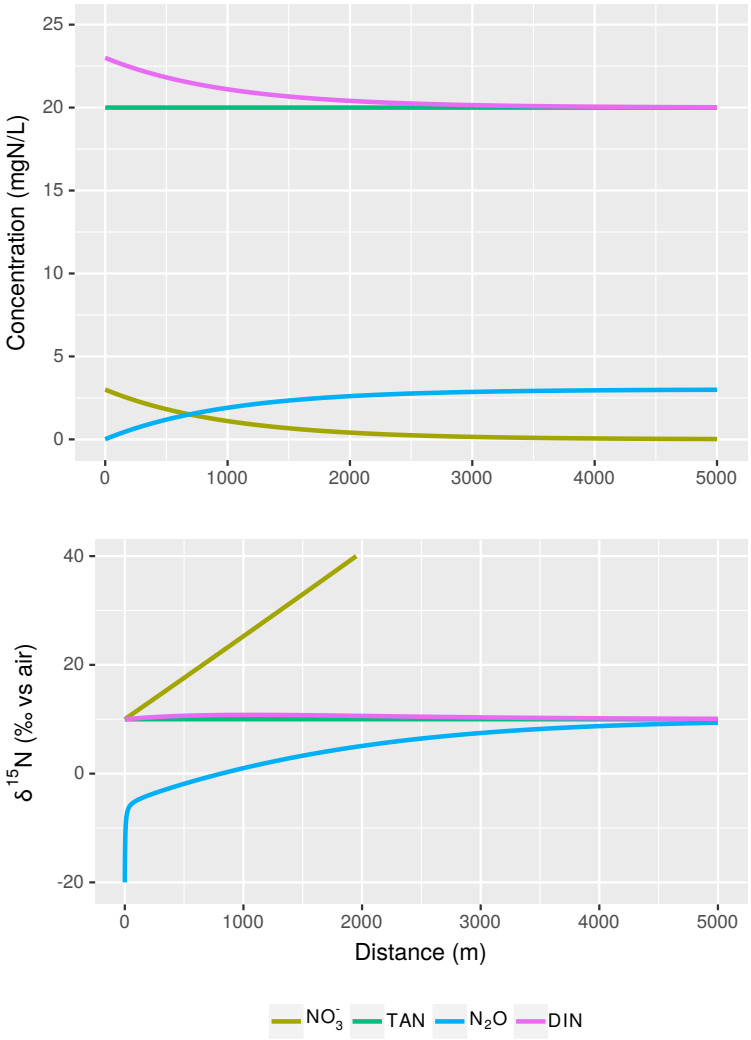

Figure S8: Each process imparts a different pattern in concentration and δ^{15}N values downstream of a WWTP discharge point in the *six-state model*. Here, denitrification only with $k_{denit} = 0.001$ and $\alpha_{denit} = 0.985$. Initial conditions as per Figure S5.

3 Tables

Table S1: Nitrogen loading to the Grand River from Waterloo (National Pollutant Release Inventory (NPRI) ID: 7649, Ontario Ministry of the Environment (ON MOE) ID:7660) and Kitchener (NPRI ID: 7645, ON MOE ID:7657) WWTPs. Data are from Environment Canada's NPRI, https://www.ec.gc.ca/inrp-npri/.

	TAN (t/yr)	NO_3^- (t/yr)	TAN:NO_3^-
Waterloo WWTP 2007	171	174	0.98:1
Waterloo WWTP 2008	135	170	0.79:1
Kitchener WWTP 2007	572	36	15.9:1
Kitchener WWTP 2008	511	77	6.6:1

Table S2: Sampling locations in the Grand River, Ontario, Canada downstream of the Waterloo (W) and Kitchener (K) waste-water treatment plants. Note that W1 and K1 are the point at which the waste-water treatment plants discharge into the river and not the plants themselves.

Site Name	Latitude	Longitude	Distance (km)
W1	43.479485	-80.482237	0
W2	43.478736	-80.481541	100
W3	43.477498	-80.479930	312
W4	43.473420	-80.472695	1062
W5	43.477190	-80.455329	2974
W6	43.477844	-80.444003	3386
W7	43.480138	-80.437432	4436
W8	43.482259	-80.431143	4911
K1	43.400944	-80.420062	0
K2	43.400270	-80.417942	200
K3	43.393846	-80.412593	1070
K4	43.397099	-80.401040	2050
K5	43.399017	-80.394399	2890
K6	43.398989	-80.386458	3970
K7	43.392486	-80.386788	4870
K8	43.384726	-80.384769	5500

Table S3: Modelled best fit solution for Waterloo 2007 for the six-state model. Results include sensitivity, identifiability, and 95% confidence intervals.

Parameter	Best-fit value	Sensitivity	Identifiability	95% confidence
k_{nit1}	3.64×10^{-7}	0.00408	0.00278	$>100\%$
k_{denit}	1.27×10^{-10}	0.0985	0.440	$>100\%$
k_{amup}	0.00439	4.61	20.6	$\pm6.83\%$
α_{nit1}	0.989	0.00291	0.00118	$>100\%$
α_{denit}	0.985	0.0000917	0.000226	$>100\%$
α_{amup}	0.990	3.21	10.1	$\pm9.70\%$

Table S4: Modelled best fit solution for Waterloo 2008 for the six-state model. Results include sensitivity, identifiability, and 95% confidence intervals.

Parameter	Best-fit value	Sensitivity	Identifiability	95% confidence
k_{nit1}	5.42×10^{-5}	0.107	0.0587	$>100\%$
k_{denit}	6.38×10^{-5}	0.135	0.716	$\pm51.7\%$
k_{amu}	0.000131	2.22	11.7	$\pm12.3\%$
α_{anit1}	0.975	0.0750	0.0294	$>100\%$
α_{adenit}	1	0.0956	0.358	$\pm73.4\%$
α_{aamup}	1	1.57	5.89	$\pm17.3\%$

Table S5: Modelled best fit solution for Kitchener 2007 for the six-state model. Results include sensitivity, identifiability, and 95% confidence intervals.

Parameter	Best-fit value	Sensitivity	Identifiability	95% confidence
k_{nit1}	0.000228	0.704	3.72	±4.34%
k_{denit}	0.000132	0.164	0.821	±11.4%
k_{amup}	0.000132	0.369	0.296	±20.8%
α_{nit1}	1.00	0.382	1.53	±8.25%
α_{denit}	0.975	0.0000414	0.0000796	> 100%
α_{amup}	0.978	0.347	1.77	±21.8%

Table S6: Modelled best fit solution for Kitchener 2008 for the six-state model. Results include sensitivity, identifiability, and 95% confidence intervals.

Parameter	Best-fit value	Sensitivity	Identifiability	95% confidence
k_{nit1}	0.000169	0.578	3.06	±20.0%
k_{denit}	5.00×10^{-7}	0.0965	0.489	±55.6%
k_{amup}	0.00168	0.280	0.903	> 100%
α_{nit1}	0.991	0.307	1.38	±35.6%
α_{denit}	1.00	$< 10^{-5}$	$< 10^{-5}$	> 100%
α_{amup}	1.00	0.279	0.0235	> 100%